The Structure of Metal-water Interface at the Potential of Zero Charge from Density Functional Theory-based Molecular Dynamics

Jiabo Le, Angel Cuesta, Jun Cheng

PII: S1572-6657(17)30623-9
DOI: doi: 10.1016/j.jelechem.2017.09.002
Reference: JEAC 3496

To appear in: *Journal of Electroanalytical Chemistry*

Received date: 8 June 2017
Revised date: 29 August 2017
Accepted date: 3 September 2017

Please cite this article as: Jiabo Le, Angel Cuesta, Jun Cheng, The Structure of Metal-water Interface at the Potential of Zero Charge from Density Functional Theory-based Molecular Dynamics, *Journal of Electroanalytical Chemistry* (2017), doi: 10.1016/j.jelechem.2017.09.002

The Structure of Metal-water Interface at the Potential of Zero Charge from Density Functional Theory-based Molecular Dynamics

Jiabo Le,[1] Angel Cuesta,[1] and Jun Cheng[1,2,*]

[1]*Department of Chemistry, University of Aberdeen, Aberdeen AB24 3UE, United Kingdom*

[2]*State Key Laboratory of Physical Chemistry of Solid Surfaces, iChEM, College of Chemistry and Chemical Engineering, Xiamen University, Xiamen 361005, China*

(Dated: September 6, 2017)

Abstract

We simulated a series of transition metal-water interfaces, namely Pt(111), Au(111), Pd(111) and Ag(111), by density functional theory based molecular dynamics, and found some common structural features for the surface water on different transition metal surfaces. Firstly, there exists a pronounced adsorption layer within ∼5 Å distance from metal surfaces , in which three main water species with different orientations (watA, watB-down and watB-up) could be identified. WatA and watB-down show a lower degree of hydrogen bonding, due to their interaction with the metal surface via one of the lone pairs of the oxygen atoms and via one of their H atoms, respectively. While, watB-up has an almost full coordination shell, indicating it not only forms hydrogen bonds in the adsorption layer, but also with the non-surface water. As expected, the honeycomb-like bilayer model used as the starting point of the simulation was destructed into irregular patterns after ∼10 ps of molecular dynamics simulations, and the surface water coverage concomitantly increases from 0.66 ML to ∼0.8 ML.

INTRODUCTION

Roger Parsons's contributions to our understanding of the electrical double layer are certainly among those for which he is best know.[1] Aqueous electrolytes are by far the most frequent, and can therefore be consider as archetypal in electrochemistry. The interaction between water and metal directly affects important interfacial processes, such as corrosion and electrocatalysis. Therefore, metal-water interfaces have drawn tremendous attention, and have been extensively studied by both experimental and computational techniques, particularly for some noble metals that can be considered as model surfaces (e.g., Pt and Au single-crystal electrodes).

Early low energy electron diffraction (LEED)[2, 3] patterns and later scanning tunneling microscopy (STM)[4–6] images of transition metal surfaces like Ru(0001) in ultra-high vacuum (UHV) at cryogenic temperatures, were interpreted in terms of a $\sqrt{3} \times \sqrt{3}$ honeycomb bilayer structure. This bilayer structure was also confirmed later by density functional theory (DFT) calculations[7–11]. The water molecules in the bilayer model are arranged in two planes separated ca. 1 Å from each other. In the bottom layer, the oxygen atoms of the water molecules are bound to the metal surface and their H atoms are slightly tilted up; in the upper layer, one of the O-H bonds is parallel to the metal surface, while the other O-H bond can point either to (H-down) or away from (H-up) the surface. For most transition metal surfaces, these two bilayer models are very similar in energetics.

However, Held and Menzel[12] found, using LEED I-V (in which the dependence of the intensity of LEED spots on the electron beam energy is analysed) to study the structure of water on Ru(0001) in UHV at cryogenic temperatures, that the oxygen atoms in the bilayer are almost co-planar, which is in contradiction with the height separation of ca. 1 Å in the honeycomb bilayer model. Based on these and other experimental results, as well as on his own DFT calculations, Feibelman[13] proposed a half dissociated H_2O-OH model on Ru(0001), which not only preserves the hexagonal rings observed in LEED and STM, but also satisfies the condition that the oxygen atoms stay in the same plane. In recent years, adsorption of water according to Feibelmann's model has been confirmed with STM on Ru(0001)[14] and Cu(110)[15]. Dissociation of surface water on Ru(0001) was also observed during density functional theory-based molecular dynamics (DFT-MD)[16]. In contrast, water dissociation is not expected on more noble metal surfaces, such as Pt(111),

as confirmed by x-ray photoelectron spectroscopy (XPS)[17]. Using high-resolution STM and DFT calculations, respectively, Nie et al.[18] and Feibelman et al.[19] revealed that water does not adsorb on Pt(111) adopting the honeycomb bilayer structure, but $\sqrt{37}$ and $\sqrt{39}$ periodic arrangements. The whole periodic structure contains a mixture of pentagonal, hexagonal and heptagonal patterns.

Unfortunately, the electron spectroscopies characteristic of UHV-based surface science are not applicable to the study of electrochemical interfaces. Although in the latter case the interfacial structure can be interrogated using techniques such as surface-enhanced infrared absorption spectroscopy in the attenuated total reflection mode (ATR-SEIRAS)[20, 21], surface X-ray scattering (SXS)[22, 23] or in situ STM[24, 25], elucidation of the structure of interfacial water is still a challenge, due to its high mobility and its complicated hydrogen bonding network.

Computational simulations offer an alternative route to obtaining microscopic information of the structures of metal-water interfaces. In the early studies, due to the limited computational resources, metal-water interfaces were mostly simulated using classical MD, in which parameterized potentials were derived from semi-empirical or ab-initio calculations [26–31]. The investigations with classical MD have indicated that the surface water layer has a prominent peak (< 5 Å) in the oxygen density profile along the surface normal near an uncharge metal electrode[27–29, 32, 33], which agrees with the experimental results from the pioneering work of Toney and co-workers[34]. However, the parameterized potentials can only provide a very approximated description for electronic interaction between metal and water, and more significantly, the charge rearrangement at the interface is generally omitted. This can lead to errors in description of metal-water interfaces, for instance, the dipolar ordering at the mercury-water interface was overestimated[31], and as a result, the potential drop across the interface was incorrectly predicted.

The recent advancements in the computer power and algorithm have allowed us to simulate the metal-water interface at an ab initio level with a comparable amount of simulation time. Since the first application of DFT-MD by Price and Halley[35] to simulate a water-metal interface in 1995 (in which the water-water interaction was still controlled by empirical parameters), this has become an important and complementary method to study the properties of metal-water interfaces, like the potential profile across the interface[36–39], the interfacial water structure[7, 16, 40–44] and the vibrational spectrum of interfacial

water[7, 44–46]. DFT-MD has also been extensively used to investigate oxide-water interfaces including mineral interfaces, for example, calculating band alignment, surface acidities, etc.[47–54].

A large fraction of recently published work involving DFT-MD simulations of transition metal-water interfaces were performed at the generalised gradient approximation (GGA) level[7, 16, 37, 39–42, 44, 55–57]. Some key findings are summarized as follows. Firstly, the ice-like bilayer water model can not stably exist at the room temperature, which has been confirmed repeatedly by several studies[7, 16, 39, 42]. Secondly, water shows a layered structure close to metal surfaces (< 5 Å), and in some cases it can be divided into two sub-layers with different water orientations[42, 44, 57]. Thirdly, due to the presence of the metal surfaces, the hydrogen bond number of interfacial water is less than that of the bulk water[16]. Given the progress that has been made from DFT-MD simulations, there however are still many issues yet to be resolved before a full picture of the interface structures can be obtained. The relatively short time scale and limited supercell size are two obvious shortcomings of the DFT-MD simulations, and insufficient sampling of the interfacial water could significantly affect simulation results on structures and interface potentials. As showed by Schnur and Gross[7], the interfacial potential change obtained from the 'H-down' and 'H-up' ice-like bilayer structures can differ by more than 2 eV. Our recent work [38] has computed the potentials of zero charge of several transition metals with a good accuracy within a time scale of $\sim$10 ps, indicating the DFT-MD time scale and model size seem adequate to converge the potential profiles at neutral metal-water interfaces. While, water structures from simulations appear more subtle. For example, dispersion correction methods in density functionals can have important impact on computed water density and orientation distributions[39, 44]. Michaelides and co-workers[58, 59] have summarized calculation results using various GGA and dispersion corrected GGA functionals[60–65] for water clusters, liquid water, and metal-water interfaces, which can be used as a general guide for choosing appropriate dispersion correction schemes. Furthermore, hydrogen bonding of interface water is still not clear. Large extended 2-D hydrogen bonding networks have been observed on Pt(100) and Pt(111) with classical MD simulations[33], while validation from ab initio calculation is lacking.

In this work, we studied the structures of water on four extensively investigated metal surfaces, namely, Pt(111), Au(111), Pd(111) and Ag(111). We employed PBE-D3 functional,

because PBE[66] has been shown to be very successful in solid-state physics[67–69], and because the combination with Grimme's D3 method[62] has also been proved effective from the calculations of various systems[56, 59, 68]. Detailed computational setup is given in the next section. The discussion section is composed of three parts: first, we analysed the distribution of water in metal-water interfaces, and characterize three configurations (watA, watB-up and watB-down). Then, we explored the hydrogen bonding network in interfacial water, including water dissociation at the surface and how water exchanges between surface and non-surface. Finally, we selected some representative snapshots of metal-water interfaces from DFT-MD trajectories, and proposed a schematic model to illustrate three different types of water configurations and their hydrogen bonding networks at the interfaces.

COMPUTATIONAL METHODS AND PRELIMINARY TESTS

Ab initio simulations were carried out using freely available CP2K/Quickstep[70]. The DFT implementation is based on a hybrid Gaussian plane wave (GPW) scheme, the orbitals are described by an atom centered Gaussian-type basis set, and an auxiliary plane wave basis set is used to re-expand the electron density in the reciprocal space. A matrix diagonalization procedure was used for the wave function optimisation and the self-consistent field (SCF) convergence was facilitated by Fermi smearing with the electronic temperature of 300 K. The 2s, 2p electrons of O, 5d, 6s electrons of Pt, 5d, 6s electrons of Au, 4s, 4p, 4d, 5s electrons of Pd and 4d, 5s electrons of Ag were treated as valence, the rest core electrons were represented by Goedecker-Teter-Hutter (GTH) pseudopotentials[71, 72]. The Gaussian basis set was double-ζ with one set of polarisation functions (DZVP)[73], the energy cutoff was set to 400 Ry. We employed PBE functional[66] to describe the exchange-correlation effects, and the dispersion correction was applied in all calculations with the Grimme D3 method[62]. The geometries were optimised by BFGS minimiser.

The lattice constant (a) was optimised by $6\times6\times6$ bulk models for each metal, containing 864 atoms in total. As shown in Table 1, the calculated lattice constants are in good agreement with experimental values for all metals, with the error bar less than 2%. Then, Pt(111) and Au(111) were modelled by $p(6\times6)$ supercell slabs with 4 atomic layers, Pd(111) and Ag(111) were modelled by $p(4\times4)$ supercell slabs with 5 and 6 atomic layers, respectively. The vacuum space between the slabs is 21 Å and full periodic boundary conditions (PBC) are

applied. The super cell sizes for Pt(111), Au(111), Pd(111) and Ag(111) are 16.869×16.869×27.887 Å^3, 17.607×17.607×28.188 Å^3, 11.059×11.059×30.030 Å^3 and 11.568×11.568×32.807 Å^3, respectively. Note that due to the large size of the interface models, only Γ point was used in all calculations.

The metal slab models in vacuum were tested by calculating their work function (Φ) and water monomer adsorption energy (E_{ads}). As shown in Table I, the calculated Φ of metal surfaces reproduces well the experimental results[74]. The only exception is Pd(111), which shows a deviation of 0.5 eV, in line with previous work[39]. This can be attributed to the functional error in the Fermi energy of Pd(111) surface. For the calculations with a water monomer, we found that water prefers to stay on a top site, and that the angles (α) formed between the water plane and the metal surfaces are very small, indicating that water stays nearly flat on the metal surfaces. The computed E_{ads} has been compared to previous simulations with dispersion correction[58], the uncertainties are within 0.1 eV. The Pt(111) and Pd(111) show higher affinity for water monomer than Au(111) and Ag(111), which is consistent with the simulation results that water stays closer to the surface of Pt(111) and Pd(111) than to that of Au(111) and Ag(111) (see below).

The metal-water interfaces were modelled by fully filling the vacuum space between the slabs with water molecules, with water density set to 1 g/mL. Thus, the Pt(111)- and Au(111)-water interfaces contain 144 metal atoms and 151 H_2O molecules, the Pd(111)-water interface contains 80 Pd atoms and 68 H_2O molecules, and the Ag(111)-water interface contains 96 Ag atoms and 69 H_2O molecules. The initial surface water configurations on Pt(111) and Au(111) were set to be H-down bilayer with 2/3 coverage. We did not choose H-up bilayer following Ogasawara et al.[17], who reported that only the signal of H-down water is observed on Pt(111) in XPS. The rest of the water molecules were pre-equilibrated with classical MD simulations for ∼100 ps. We used a randomised initial structure with a coverage of 3/4 for the surface water molecules on Pd(111) and Ag(111), because the $p(4\times4)$ surfaces do not have the symmetry of the $\sqrt{3}\times\sqrt{3}$ water bilayer. The other water molecules were dealt in the same way as on Pt(111) and Au(111). To rule out the effect of finite size error on the structure of interfacial water, we have compared the water density distribution computed from $p(4\times4)$ and $p(6\times6)$ surfaces of Pt(111), which is shown in our previous publication[38].

Then, we ran Born-Oppenheimer DFT-MD with a time step of 0.5 fs. The canonical

ensemble condition was imposed by a Nose-Hoover thermostat (NVT) with a target temperature of 330 K. The first 3 ps of the simulations were regarded as the equilibration period, followed by production periods of 10, 6, 10 and 15 ps for Pt, Au, Pd and Ag models, respectively. To compare with interfacial water, we also simulated bulk water by calculating a cubic box of $9.86 \times 9.86 \times 9.86$ Å^3, containing 32 water. All the settings are same as stated above, the production period is 30 ps.

No net charges or counter ions were introduced at the metal-water interfaces in our model. Therefore, our simulations correspond to the interfacial structures of water at the potential of zero charge (PZC). We have recently reported values of the PZC calculated using our DFT-MD model for the metal-water interfaces studied here, which were in good agreement with experimental values[38].

RESULTS AND DISCUSSION

Water distribution

The structures of metal-water interfaces are often characterized by their water density (ρ_{H_2O}) and dipole-orientation ($\rho_{H_2O}\cos\Psi$, where Ψ is the angle between water bisector and surface normal, as shown in the inset of Figure 1(b)) distribution functions. These are shown in Figure 1, as averaged from DFT-MD trajectories, for Pt(111), Au(111), Pd(111) and Ag(111). Figure 1(a) reveals the presence of a water layer in the region between ca. 2 and 5 Å away from the metal surface for all the investigated systems, which coincides with the water distribution profile interpreted from the experimental results of Toney et al.[34]. The averaged density of this layer, as obtained from the distribution function, is 1 g/mL, in line with the results of Nadler et al.[44] for the Au-water interface.

Figure 1(b) shows that this surface water layer can be regarded as a 'bilayer' structure (N.B. not the ice-like honeycomb bilayer structure) composed by two parts with opposite net orientation dipoles. We denote the sub-layer closer to the surfaces as watA, which has a positive , and the other as watB, having a negative $\cos\Psi$. The watA sub-layers are closer to the surfaces of Pt(111) and Pd(111) at a distance < 2.8 Å, than Au(111) and Ag(111) at a distance < 3.0 Å. The dipole orientation indicates that water molecules in watA adopt an 'O-down' configuration. The watB sub-layer is adjacent to watA, up to a

distance of 4.6 Å for Pt(111) and Pd(111), and 5.0 Å for Au(111) and Ag(111). The net dipole orientation $\rho_{H_2O}\cos\Psi$ of watB is negative, which indicates water with a 'H-down' configuration dominates in this region.

In order to determine how many types of water configurations exist in the surface water bilayer, we performed a distribution analysis for the angle between the water bisector and the surface normal (Ψ), and for the angle between the O-H bond and the surface normal (θ), as shown in Figure 2 and Figure 3, respectively. In Figure 2(a), we found that the distribution angle Ψ of watA presents only one main peak for all studied interfaces, located at 60°. This type of angle distribution indicates that watA only has one main configuration on all these transition metal surfaces. The θ distribution profiles in Figure 3(a) also show a single peak for all systems, located at 70°, which again indicates that there is only one main pointing direction of the O-H bond. Combining both angle distributions, we conclude that watA is adsorbed on metal surfaces with an 'O-down' configuration and the two O-H bonds almost symmetrically tilted up. Moreover, the angles of watA on Pt(111) and Pd(111) are distributed in narrower regions than on Au(111) and Ag(111) for both angle distributions, suggesting watA is more flexibly oriented on Au(111) and Ag(111) than Pt(111) and Pd(111). This must be attributed to stronger chemisorption on Pt(111) and Pd(111) than on Au(111) and Ag(111).

In contrast, there are two main peaks in the Ψ distribution for watB, at 50° and 130°, respectively, as shown in Figure 2(b), the latter being dominant for all investigated interfaces. Furthermore, three peaks are found in the θ distribution in Figure 3(b), at 20°, 100° and 155°, respectively. It is interesting to see comparable number of O-H bonds pointing almost vertically to ($\theta \approx 20°$) and away of ($\theta \approx 160°$) the metal surface, though the majority of the O-H bonds are nearly parallel to the metal surface ($\theta \approx 90°$). We interpret the peaks close to 50° and 130° in Figure 2(b) as watB-down and watB-up configurations, respectively, similar to the 'H-down' and 'H-up' water molecules in the honeycomb-like bilayer models[7, 9]. A third fraction, watB-para, would correspond to water molecules with both O-H bonds roughly parallel to the metal surface, following the definition of Velasco-Velez and co- workers[56], with angles within 60° and 120° from the surface normal. By integrating the O-H bond population in the $60° < \theta < 120°$ region in Figure 3(b), we found it occupies around 50% of the total O-H bonds, and the other 50% is either pointing to or away from the metal surface, the number of which almost coincides with the total of watB-up and watB-down

water molecules integrating the two peaks around 20° and 160°. Therefore, we conclude that watB-para is just a minor population, and the watB layer is a mixture of watB-up and watB-down, with the latter more abundant.

The average number of the surface water molecules (N_{surf}) was obtained by integrating the water density distribution function within z < 5 Å in Figure 1(a). The surface coverage (γ) can be then obtained dividing N_{surf} by the number of surface metal atoms (N). Values of N_{surf} and γ are listed in Table II for all the interfaces studied. γ fluctuates around 0.8 ML, clearly higher than the surface coverage of the ice-like honeycomb bilayer model (0.66 ML). We also calculated the average number of water molecules in the watA (N_{watA}) and watB (N_{watB}) layers. Interestingly, the N_{watA} to N_{watB} ratio is around 1 : 3 for all the metal-water interfaces studied. We also calculated the average angle between the plane of the water molecules in watA and the metal surface, also listed in Table II. The angles are either around 15° (Au(111) and Ag(111)) or 26° (Pt(111) and Pd(111)), nearly twice the corresponding angles calculated for a single adsorbed water molecule in vacuum (Table I). The increase of the angle must be due to intermolecular hydrogen bonding with other surface water molecules, as will be discussed below.

Hydrogen bonding

Back to the water density distribution function (Figure 1), the surface water 'bilayer' was found to be followed by a valley in the region between 4 and 6 Å. Similar low-density regions were also observed in previous classical MD[27, 28, 31, 33, 75] and DFT-MD[39, 44, 55, 56] simulations of metal-water interfaces. The existence of this region is generally explained by the formation of 2-D hydrogen bonding networks in surface water[33, 75]. It is therefore relevant to study hydrogen bonding within the interfacial water bilayer. Figure 4 shows plots of the O-O radial distribution functions ($g_{OO}(r)$) for different kinds of water on all four surfaces studied. $g_{OO}(r)$ provides information regarding the solvation shell around each water molecule. The black lines in Figure 4 correspond to bulk water, as calculated using a 32-water model, considered a benchmark model for computing bulk water[59, 76, 77]. No distinct differences can be found in the peak position of the first and the second solvation layers between our computed $g_{OO}(r)$ for bulk water and those of other published works using the PBE-D3 method[77].

We denote the water molecules in the region at z > 7 Å of our interfacial models as watC. They are less affected by the metal surfaces, and similar to bulk water, with density ≈ 1 g/mL and no obvious net orientation, as shown in Figure 1. There exists a slight difference, though, between $g_{OO}(r)$ of watC and that of bulk water for all computed systems, suggesting that the structure and dynamics of watC are still affected by the metal surface in our nano-sized water region. This agrees with the findings of Velasco-Velez et al.[56] and Limmer et al.[33, 75] that the thickness of the interfacial water is of approximately 1 nm. The first $g_{OO}(r)$ peak of surface water shows a significantly lower intensity than that of watC and bulk water, but it appears at roughly the same value of r, i.e., the coordination number of surface water is lower, but the O-O distance does not change. This suggests that the presence of the metal surface partially strips water from the first solvation layer, but the interaction between water and the metal surface does not apparently affect the degree of hydrogen bonding with the remaining solvation layer. Integration of the first peak of the $g_{OO}(r)$ function yields the coordination number. Surface water, watC and bulk water are surrounded by 3.1, 3.8 and 3.8 water molecules, respectively, for all computed interfaces. The difference between the coordination number of surface water and that of bulk water (0.7) suggests that the metal surface roughly occupies one of the hydrogen bonds available in the surface water molecules. A similar decrease of the coordination number of surface water was also observed in other studies[16, 44, 78].

In order to investigate further the interfacial hydrogen bonding network, we analysed the average hydrogen bond number distribution along the surface normal, as displayed in Figure 5. Following Velasco-Velez et.al.[56] and Cicero et.al.[78], a hydrogen bond is assumed to be present if the O-O distance is shorter than 3.5 Å and the O-O-H angle less than 35°. The black lines in Figure 5 represent the total number of hydrogen bonds formed by each water molecule along the surface normal, and confirm the finding from our $g_{OO}(r)$ analysis that the hydrogen bond number for surface water is 3, while it is 4 for watC (z > 7 Å). We split the hydrogen bonds population into two types, Donor and Acceptor, whereby Donor donates H atoms and Acceptor accepts H atoms. As shown in Figure 5, Donor (red line) and Acceptor (blue line) populations present similar distributions within the watC region, but its distribution is considerably different in the surface water layer. For all computed metal-water interfaces, each water molecule in the watA region donates ∼2 H atoms and accepts ∼1 H atom, while in the watB region, the Acceptor population becomes dominant.

We then calculated the average number of hydrogen bonds per water molecule within each region. The results are shown in Table III. Combined with the result that within watA the H atoms are pointing away of the metal surface, we conclude that watA donates two H to neighbouring water molecules. One of its oxygen lone pairs receives a H from another water molecule, while the other lone pair interacts with the metal surface[79]. The top site of the metal surface is the most likely place to find watA, which agrees with the most stable adsorption site of water monomer in vacuum (see Table I) and with the DFT-MD snapshots in Figure 6. As discussed above, the average angle between the molecular plane of watA and the metal surface (α_{watA}) is nearly twice as large as that of an adsorbed water monomer in vacuum. We attribute this increase to hydrogen bonding with neighbouring molecules in the case of interfacial water.

For watB, the average number of hydrogen bonds per molecule is 3.4, which is in between those of watA and watC. As discussed above, watB has two main configurations, watB-up and watB-down. WatB-down forms just 3 hydrogen bonds, as expected, because the O-H bond pointing to the metal surface cannot act as a donor to another water molecule. The average number of hydrogen bonds of watB-up is 3.6, which implies that the O-H bond pointing away from the metal surface can also form a hydrogen bond with the water above the adsorption layer, i.e. non-surface water. The ratio of watB-up and watB-down depends on the the metal surface. The relative population of watB-up and watB- down was obtained by integrating the regions of $\Psi < 90$ and $\Psi > 90$ in Figure 2, respectively. The watB-up : watB-down ratio is around 1 : 2 for Pt(111) and Pd(111), while for Au(111) and Ag(111) it is around 1 : 1.5, i.e., on Pt(111) and Pd(111) there is a slightly higher preference for the watB-down configuration than on Au(111) and Ag(111).

Interface Models

In order to illustrate the structures of interfacial water, we selected one representative configuration from our DFT-MD trajectories for each interface (Figure 6). The snapshots show that the pre-set ice-like honeycomb patterns on Pt(111) and Au(111) have become destructed, and no new ordered structure has formed on any of the metal surfaces, in consistent with the previous work[7, 16, 39, 42]. Surface water can be categorized into watA (blue balls) and watB (red balls), and the estimate surface coverage is $\sim$0.8 ML. WatA is

primarily located at on-top or near-on-top sites on Pt(111) and Pd(111), while on Au(111) and Ag(111) some watA molecules are located on other sites, confirming that watA is more strongly bound on Pt(111) and Pd(111) than on Au(111) and Ag(111). Interestingly, watA tends to form local clusters on Pt(111), similar to the "Y" shaped dark regions observed by Feibelman et al.[18, 19] using high resolution STM in UHV conditions. The number of watB molecules is about three times of the watA number, and watB does not show preference on adsorption sites, as can be seen from Figure 6. This finding is different from classical MD simulations [33, 75], in which, almost all surface water bind on the top sites at the Pt-water interface. The snapshots in Figure 6 also confirm our interpretation of the degree and distribution of hydrogen bonding within interfacial water. As discussed above, most watA molecules donate two hydrogen bonds and receive one. The hydrogen bonding network is incomplete for watB in Figure 6 since only the adsorption water layer is shown with the rest water removed for clarity. We find that watB-up receives two hydrogen bonds and its surface-parallel O-H donates a hydrogen bond to a neighbouring water in the adsorption layer. It is clear that the perpendicular O-H bond forms a hydrogen bond with a non-surface water, although it is not shown. For most of watB-down molecules, they donate one hydrogen bond and receive two, in which one water donor comes from the non-surface water.

In the end, we sketch a rather simplified illustration of surface water structure in Figure 7, obtained from our DFT-MD simulations of four transition metal-water interfaces, to summarize some key features. Firstly, the metal-water interface in Figure 7 is represented by five metal atoms (grey balls) and four water molecules (blue and red balls), indicating a surface coverage of $\sim$0.8 ML. Secondly, the surface water can be decomposed into two sub-layers, watA (blue) and watB (red). The watA stays closer to the metal surface, and is usually located on the top sites. Both of its O-H bonds are slightly tilted up to form hydrogen bonds with neighboring water. Thirdly, there are two main configurations in the sub-layer above (watB-up and watB-down) and the estimate ratio is approximately 1 : 2. WatB-up has one O-H forming a hydrogen bond with non-surface water, and watB-down has a O-H bond pointing directly towards the metal surface. The rest O-H bonds lying roughly parallel to the surface, together with the O-H bonds of watA, constitute the hydrogen bond network within the surface water layer. Finally, given the diverse configurations and orientations of surface water, the overall orientation dipoles of the surface water layers are rather small at

neutral transition metal-water interfaces.

CONCLUSIONS

This work provides some new insight into the microscopic water structure on metal electrodes at the PZC. Based on DFT-MD simulations of four commonly studied metal-water interfaces, namely, Pt(111), Au(111), Ag(111) and Pd(111), we are able to unravel some general features of the structure of the interfacial water on close-packed transition metal surfaces:

i) Interfacial water presents a layered structure with a thickness of ca. 5 Å. The $\sqrt{3} \times \sqrt{3}$ hexagonal structure with the ice-like honeycomb bilayer is not present at 330 K. The surface coverage at the metal-electrolyte interface is ∼0.8 ML, higher than that of the ice-like water bilayer often found in UHV.

ii) Three water populations with different configurations, watA, watB-up and watB-down, were identified within the interfacial water layer. WatA adsorbs on the metal surface via O atom with its H atoms pointing away from the surface. The adjacent watB-up and watB-down have one O-H bond parallel to the metal surface, and the other O-H bond points to the liquid water and the metal surface, respectively.

iii) WatA and watB-down only form three hydrogen bonds, losing around one coordination number compared to bulk water due to the interaction with the metal surface (M-OH_2 and M-HOH modes, respectively). watB-up is almost fully coordinated, which indicates there is a hydrogen bonding interaction with non-surface water.

iv) There are clear structural differences between two relatively inert surfaces, namely, Au(111) and Ag(111), and two more reactive surfaces, namely, Pt(111) and Pd(111). Pt(111) and Pd(111) show a higher affinity for watA and watB-down than Au(111) and Ag(111).

ACKNOWLEDGEMENTS

J. Le thanks the College of Physical Sciences, University of Aberdeen for a PhD studentship. Calculations were performed on ARCHER, the UK's high end computing resource, as part of a grant to the UKCP consortium, and on the computing cluster Maxwell at the University of Aberdeen. J. C. is grateful for funding support by the National Natural Sci-

ence Foundation of China (Grants No. 21373166 and 21621091), and the Thousand Youth Talents Program of China.

* chengjun@xmu.edu.cn, jcheng@abdn.ac.uk

[1] R. Parsons, Chem. Rev. **90**, 813 (1990).

[2] P. A. Thiel, F. M. Hoffmann, and W. H. Weinberg, J. Chem. Phys. **75**, 5556 (1981).

[3] D. L. Doering and T. E. Madey, Surf. Sci. **123**, 305 (1982).

[4] T. Mitsui, M. K. Rose, E. Fomin, D. F. Ogletree, and M. Salmeron, Science (New York, N.Y.) **297**, 1850 (2002).

[5] K. Morgenstern and J. Nieminen, Phys. Rev. Lett. **88**, 066102 (2002).

[6] K. Morgenstern and K.-H. Rieder, J. Chem. Phys. **116**, 5746 (2002).

[7] S. Schnur and A. Groß, New J. Phys. **11**, 125003 (2009).

[8] K. Tonigold and A. Gross, J. Comput. Chem. **33**, 695 (2012).

[9] A. Hodgson and S. Haq, Surf. Sci. Rep. **64**, 381 (2009).

[10] J. Carrasco, A. Hodgson, and A. Michaelides, Nat. Mater. **11**, 667 (2012).

[11] V. Tripkovic, M. E. Björketun, E. Skúlason, and J. Rossmeisl, Phys. Rev. B **84**, 115452 (2011).

[12] G. Held and D. Menzel, Surf. Sci. **316**, 92 (1994).

[13] P. J. Feibelman, Science (New York, N.Y.) **295**, 99 (2002).

[14] M. Tatarkhanov, E. Fomin, M. Salmeron, K. Andersson, H. Ogasawara, L. G. M. Pettersson, A. Nilsson, and J. I. Cerdá, J. Chem. Phys. **129**, 154109 (2008).

[15] M. Forster, R. Raval, A. Hodgson, J. Carrasco, and A. Michaelides, Phys. Rev. Lett. **106**, 046103 (2011).

[16] L. Bellarosa, R. García-Muelas, G. Revilla-López, and N. López, ACS Cent. Sci. **2**, 109 (2016).

[17] H. Ogasawara, B. Brena, D. Nordlund, M. Nyberg, A. Pelmenschikov, L. G. M. Pettersson, and A. Nilsson, Phys. Rev. Lett. **89**, 276102 (2002).

[18] S. Nie, P. J. Feibelman, N. C. Bartelt, and K. Thürmer, Phys. Rev. Lett. **105**, 026102 (2010).

[19] P. J. Feibelman, N. C. Bartelt, S. Nie, and K. Thürmer, J. Chem. Phys. **133**, 154703 (2010).

[20] K.-i. Ataka, T. Yotsuyanagi, and M. Osawa, J. Chem. Phys. **100**, 10664 (1996).

[21] M. Osawa, M. Tsushima, H. Mogami, G. Samjeské, and A. Yamakata, J. Phys. Chem. C **112**, 4248 (2008).

[22] C. A. Lucas, P. Thompson, Y. Gründer, and N. M. Markovic, Electrochem. Commun. **13**, 1205 (2011).

[23] Y. Gründer, A. Drünkler, F. Golks, G. Wijts, J. Stettner, J. Zegenhagen, and O. Magnussen, Surf. Sci. **605**, 1732 (2011).

[24] M. Escudero-Escribano, G. J. Soldano, P. Quaino, M. E. Zoloff Michoff, E. P. Leiva, W. Schmickler, and Á. Cuesta, Electrochim. Acta **82**, 524 (2012).

[25] M. Escudero-Escribano, C. Wildi, J. A. Mwanda, and A. Cuesta, J. Solid State Electrochem. **20**, 1087 (2016).

[26] J. Bocker, R. Nazmutdinov, E. Spohr, and K. Heinziger, Surf. Sci. **335**, 372 (1995).

[27] E. Spohr, J. Chem. Phys. **93**, 6171 (1989).

[28] K. Raghavan, K. Foster, K. Motakabbir, and M. Berkowitz, J. Chem. Phys. **94**, 2110 (1991).

[29] K. Foster, K. Raghavan, and M. Berkowitz, Chem. Phys. Lett. **162**, 32 (1989).

[30] J. I. Siepmann and M. Sprik, J. Chem. Phys. **102**, 511 (1995).

[31] E. Spohr, in *Advances in Electrochemical Science and Engineering*, Vol. 6 (WileyVCH Verlag GmbH, 2008) pp. 1–75.

[32] E. Spohr, G. Tóth, and K. Heinzinger, Electrochim. Acta **41**, 2131 (1996).

[33] D. T. Limmer, A. P. Willard, P. Madden, and D. Chandler, Proc. Natl. Acad. Sci. **110**, 4200 (2013).

[34] M. F. Toney, J. N. Howard, J. Richer, G. L. Borges, J. G. Gordon, O. R. Melroy, D. G. Wiesler, D. Yee, and L. B. Sorensen, Nature **368**, 444 (1994).

[35] D. L. Price and J. W. Halley, J. Chem. Phys. **102**, 6603 (1995).

[36] M. Otani, I. Hamada, O. Sugino, Y. Morikawa, Y. Okamoto, and T. Ikeshoji, J. Phys. Soc. Jpn. **77**, 1 (2008).

[37] S. Sakong, K. Forster-Tonigold, and A. Groß, J. Chem. Phys. **144**, 194701 (2016).

[38] J. Le, M. Iannuzzi, A. Cuesta, and J. Cheng, Phys. Rev. Lett. **119**, 016801 (2017).

[39] L. S. Pedroza, A. Poissier, and M.-V. Fernández-Serra, J. Chem. Phys. **142**, 034706 (2015).

[40] S. Izvekov and G. a. Voth, J. Chem. Phys. **115**, 7196 (2001).

[41] S. Izvekov, A. Mazzolo, K. VanOpdorp, and G. A. Voth, J. Chem. Phys. **114**, 3248 (2001).

[42] P. Vassilev, R. A. van Santen, and M. T. M. Koper, J. Chem. Phys. **122**, 54701 (2005).

[43] S. Meng, E. G. Wang, and S. Gao, Phys. Rev. B **69**, 195404 (2004).

[44] R. Nadler and J. F. Sanz, J. Chem. Phys. **137**, 114709 (2012).

[45] X. Lin and A. Groß, Surf. Sci. **606**, 886 (2012).

[46] X. Lin, F. Evers, and A. Groß, Beilstein J. Nanotechnol. **7**, 533 (2016).

[47] J. Cheng, X. Liu, J. A. Kattirtzi, J. VandeVondele, and M. Sprik, Angew. Chem. Int. Ed. **53**, 12046 (2014).

[48] J. Cheng and M. Sprik, Phys. Chem. Chem. Phys. **14**, 11245 (2012).

[49] X. Liu, X. Lu, M. Sprik, J. Cheng, E. J. Meijer, and R. Wang, Geochim. Cosmochim. Acta **117**, 180 (2013).

[50] X. Liu, J. Cheng, M. Sprik, X. Lu, and R. Wang, Geochim. Cosmochim. Acta **120**, 487 (2013).

[51] X. Liu, J. Cheng, X. Lu, and R. Wang, Phys. Chem. Chem. Phys. **16**, 26909 (2014).

[52] J. Cheng, X. Liu, J. VandeVondele, and M. Sprik, Electrochim. Acta **179**, 658 (2015).

[53] J. Cheng and M. Sprik, Phys. Rev. B: Condens. Matter **82**, 1 (2010).

[54] J. Cheng and M. Sprik, J. Chem. Theory Comput. **6**, 880 (2010).

[55] M. Otani, I. Hamada, O. Sugino, Y. Morikawa, Y. Okamoto, and T. Ikeshoji, Phys. Chem. Chem. Phys. **10**, 3609 (2008).

[56] J.-J. Velasco-Velez, C. H. Wu, T. A. Pascal, L. F. Wan, J. Guo, D. Prendergast, and M. Salmeron, Science **346**, 831 (2014).

[57] R. Nadler and J. Fernandez Sanz, J. Mol. Model. **18**, 2433 (2012).

[58] J. Carrasco, J. Klimes, and A. Michaelides, J. Chem. Phys. **138**, 024708 (2013).

[59] M. J. Gillan, D. Alfè, and A. Michaelides, J. Chem. Phys. **144**, 130901 (2016).

[60] S. Grimme, J. Comput. Chem. **25**, 1463 (2004).

[61] S. Grimme, J. Comput. Chem. **27**, 1787 (2006).

[62] S. Grimme, J. Antony, S. Ehrlich, and H. Krieg, J. Chem. Phys. **132**, 154104 (2010).

[63] M. Dion, H. Rydberg, E. Schröder, D. C. Langreth, and B. I. Lundqvist, Phys. Rev. Lett. **92**, 246401 (2004).

[64] O. A. Vydrov and T. Van Voorhis, J. Chem. Phys. **133**, 244103 (2010).

[65] K. Lee, É. D. Murray, L. Kong, B. I. Lundqvist, and D. C. Langreth, Phys. Rev. B **82**, 081101 (2010).

[66] J. P. Perdew, K. Burke, and M. Ernzerhof, Phys. Rev. Lett. **77**, 3865 (1996).

[67] Y.-H. Fang, G.-F. Wei, and Z.-P. Liu, Catal. Today **202**, 98 (2013).

[68] Y. Yoon, R. Rousseau, R. S. Weber, D. Mei, and J. A. Lercher, J. Am. Chem. Soc. **136**, 10287 (2014).

[69] H.-F. Wang and Z.-P. Liu, J. Phys. Chem. C **113**, 17502 (2009).

[70] J. VandeVondele, M. Krack, F. Mohamed, M. Parrinello, T. Chassaing, and J. Hutter, Comput. Phys. Commun. **167**, 103 (2005).

[71] S. Goedecker, M. Teter, and J. Hutter, Phys. Rev. B **54**, 1703 (1996).

[72] C. Hartwigsen, S. Goedecker, and J. Hutter, Phys. Rev. B **58**, 3641 (1998).

[73] J. VandeVondele and J. Hutter, J. Chem. Phys. **127**, 114105 (2007).

[74] H. B. Michaelson, J. Appl. Phys. **48**, 4729 (1977).

[75] D. T. Limmer and A. P. Willard, Chem. Phys. Lett. **620**, 144 (2015).

[76] J. Wang, G. Román-Pérez, J. M. Soler, E. Artacho, and M.-V. Fernández-Serra, J. Chem. Phys. **134**, 024516 (2011).

[77] A. Bankura, A. Karmakar, V. Carnevale, A. Chandra, and M. L. Klein, J. Phys. Chem. C **118**, 29401 (2014).

[78] G. Cicero, J. C. Grossman, E. Schwegler, F. Gygi, and G. Galli, J. Am. Chem. Soc. **130**, 1871 (2008).

[79] A. Michaelides, V. A. Ranea, P. L. de Andres, and D. A. King, Phys. Rev. Lett. **90**, 216102 (2003).

TABLE I. Calculated lattice constants (a) of bulk metals, work functions (Φ), energies (E_{ads}) and structures of water adsorption on metal surfaces in vacuum. Values in the parentheses were taken from experimental results or previous theoretical work[58, 74]. The optimised water structure on metal surfaces was characterised by the distance between oxygen and its nearest metal atom (O-metal), the lateral displacement of oxygen from the top site of metal surface (ΔOxy) , and the dihedral between the molecular plane of water and the metal surface (α).

Surface	a / Å	Φ / eV	E_{ads} / eV	O-metal / Å	ΔOxy / Å	α / degrees
Pt(111)	3.98 (3.92)	5.8 (5.9)	-0.43 (-0.4)	2.34	0.11	12
Au(111)	4.15 (4.08)	5.4 (5.4)	-0.24 (-0.28)	2.79	0.02	9
Pd(111)	3.91 (3.89)	5.1 (5.6)	-0.5 (-0.42)	2.37	0.06	10
Ag(111)	4.09 (4.09)	4.7 (4.8)	-0.25 (-0.28)	2.82	0.01	6

TABLE II. Numbers of surface metal atoms (N), adsorbed water molecules (N_{surf}), watA molecules (N_{watA}) and watB molecules (N_{watB}). γ is the surface water coverage and α_{watA} is the dihedral between the molecular plane of watA and the metal surface. All the results are averaged over ∼10 ps DFT-MD trajectories.

Surface	N	N_{surf}	γ / ML	N_{watA}	α_{watA} / degrees	N_{watB}
Pt(111)	36	27.7	0.77	6.5	26	21.2
Au(111)	36	29.7	0.82	6.1	16	23.6
Pd(111)	16	12.6	0.79	3.5	26	9.1
Ag(111)	16	12.8	0.8	3.2	15	9.6

TABLE III. Average numbers of hydrogen bonds of different kinds of water on Pt(111), Au(111), Pd(111) and Ag(111). Please see the main text for definitions of watA, watB, watB-up, watB-down and watC.

Surface	watA	watB	watB-up	watB-down	watC
Pt(111)	2.74	3.21	3.66	3.01	3.80
Au(111)	2.92	3.39	3.59	3.22	3.75
Pd(111)	2.88	3.43	3.76	3.22	3.83
Ag(111)	2.9	3.39	3.57	3.18	3.89

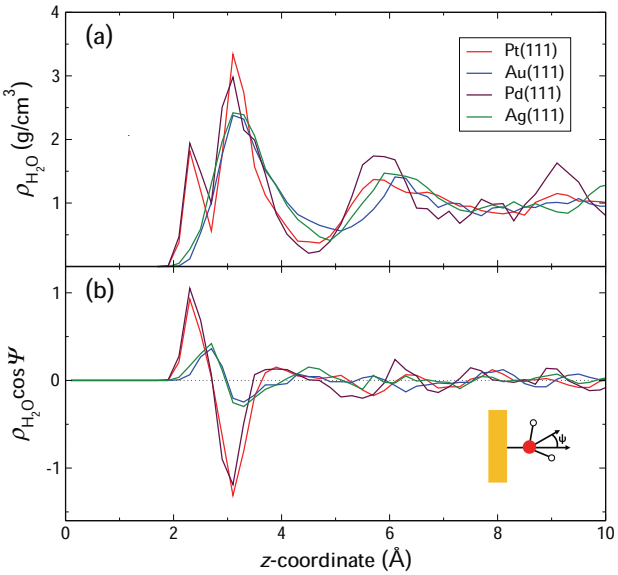

FIG. 1. Water density (a) and water-dipole orientation (b) distributions along the surface normal (average of the two symmetrical interfaces in our model). The zero coordinate corresponds to the position of the metal surface. Results corresponding to Pt(111)-, Au(111)-, Pd(111)-, and Ag(111)-water interfaces are represented by red, blue, maroon and green curves, respectively. The inset in (b) illustrates the angle Ψ between the water bisector and the surface normal.

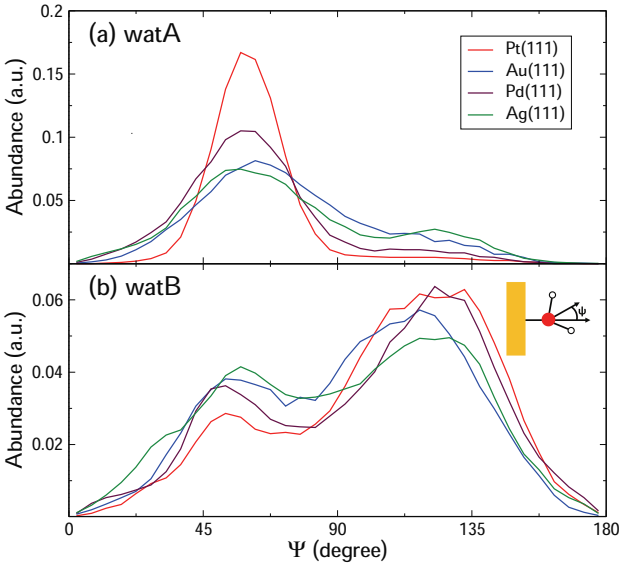

FIG. 2. Normalised distribution profiles of the angle Ψ between the water bisector and the surface normal of watA (a) and watB (b). Red, blue, maroon and green curves represent Pt(111)-, Au(111)-, Pd(111)-, and Ag(111)-water interfaces, respectively.

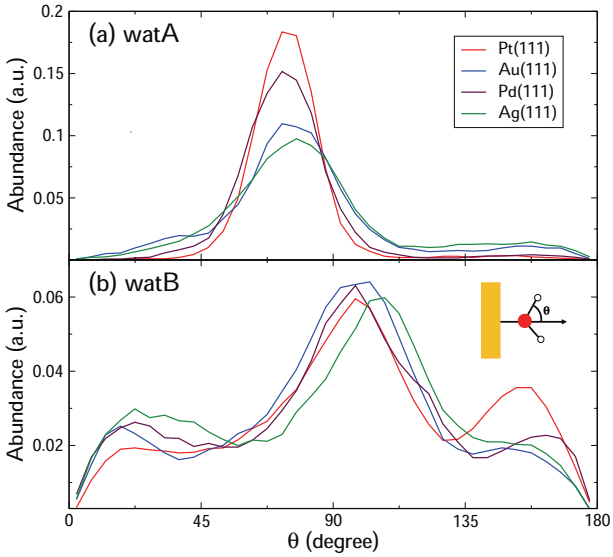

FIG. 3. The normalised distribution profiles of the angle θ between the O-H bond and the surface normal of watA (a) and watB (b). Red, blue, maroon and green curves represent Pt(111)-, Au(111)-, Pd(111)-, and Ag(111)-water interfaces, respectively.

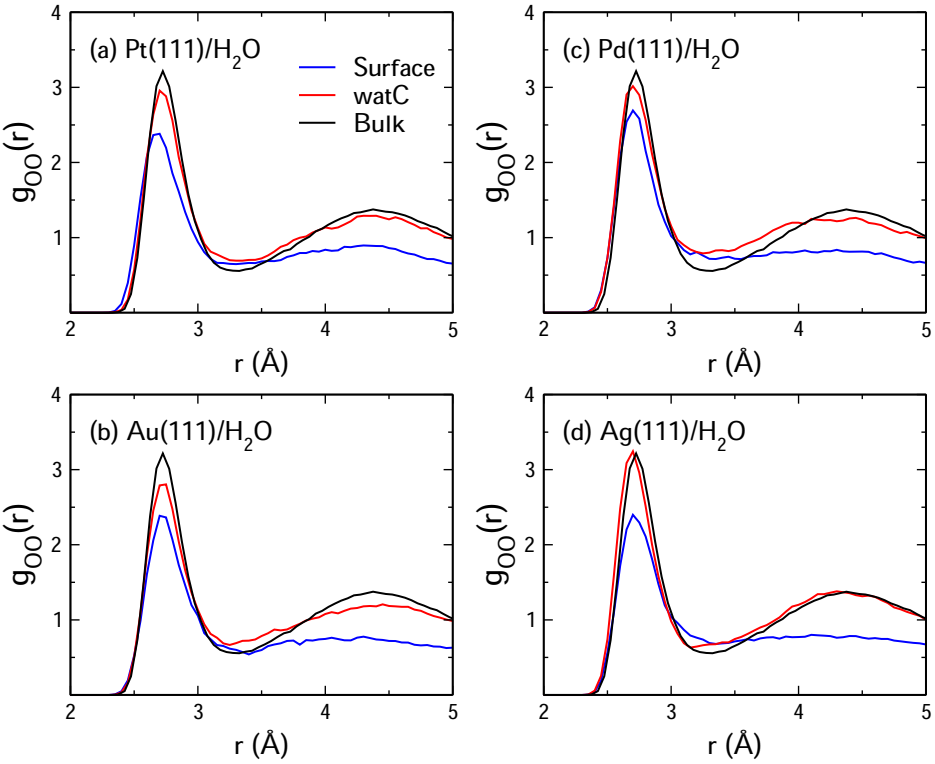

FIG. 4. Water O-O radial distribution functions (g_{OO}) at Pt(111)-, Pd(111)-, Au(111)- and Ag(111)-water interfaces in comparison with that of bulk water. The black curves correspond to bulk water, as calculated with a 32-water box. The g_{OO} of surface water and watC are denoted in blue and red, respectively.

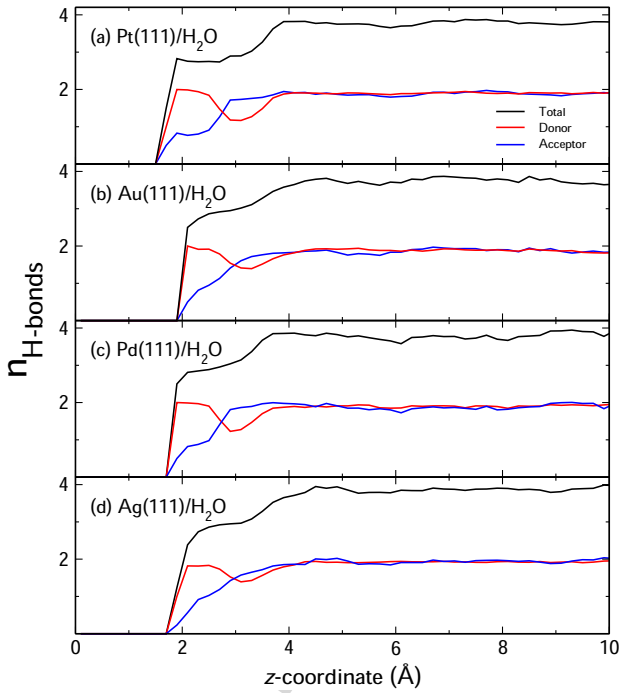

FIG. 5. Average numbers of water-water hydrogen bonds in Pt(111)-, Au(111)-, Pd(111)-, and Ag(111)-water interfacial models. It is assumed that a hydrogen bond is formed between two water molecules if the O-O distance is shorter than 3.5 Å and the O-O-H angle is less than 35°. Donor (red) means the water molecules donate a H atom when forming a hydrogen bond, while Acceptor (blue) means they accept a H atom. The black curve represents the total number of hydrogen bonds (sum of Donor + Acceptor). z = 0 corresponds to the position of the metal surface.

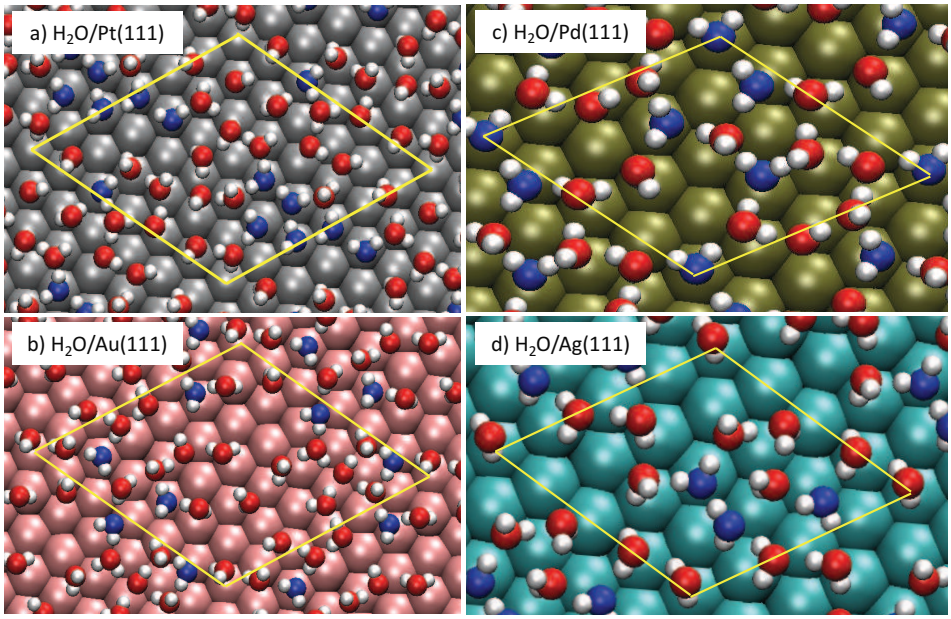

FIG. 6. Snapshots of surface water configurations on Pt(111), Au(111), Pd(111) and Ag(111), taken from DFT-MD simulations at 330 K. The water molecules with blue and red oxygen atoms represent watA and watB, respectively. The yellow parallelograms indicate the periodic super-cells.

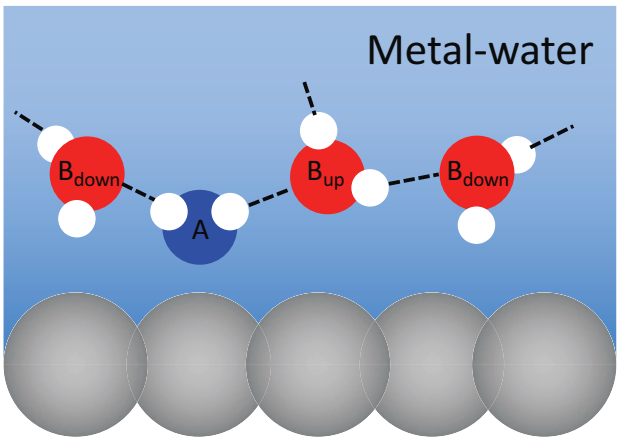

FIG. 7. Schematic illustration of the water structure at a metal-water interface. The grey balls denote the metal surface, the water molecule with blue ball represents watA, and the water molecules with red balls are a mixture of watB-up and watB-down. The dashed lines indicate the hydrogen bonds formed between water molecules.